Dynamic Rupture Along Bimaterial Interfaces in 3D

G. B. Brietzke, A. Cochard[1], and H. Igel

Department für Geo- und Umweltwissenschaften, Sektion Geophysik, Ludwig-Maximillians-Universität München, Theresientrasse 41, 80333 München, Germany

Abstract. We perform numerical simulations of dynamic rupture propagation on a plane in a model consisting of two different elastic half spaces connected via a planar frictional interface governed by regularized Coulomb friction. Therefore, ruptures in this study are purely driven by the presence of a material contrast. Ruptures are nucleated on the fault using a circular symmetric expanding increase of pore-pressure in a limited source region. We show how a wrinkle-like rupture pulse can mature also in the 3D case where we have a mixing of in-plane and anti-plane modes, the instability specific of a bimaterial interface acting only for the in-plane mode. The pulse develops inside a cone-shaped region around the in-plane direction of slip in the softer material.

[1] now at École et Observatoire des Sciences de la Terre, 5 rue René Descartes, 67084 Strasbourg Cedex, France

1. Introduction

Geological faults with a long slip history are likely to bring into contact materials with different elastic properties. Recent geologic mapping and laboratory experiments both suggest that the principal zones of slip are localized along interfaces that separate considerably different rocks [*Dor et al.*, 2006a, b]. Contrasts of elastic properties across large faults have been imaged by seismic reflection and refraction studies [*Fuis et al.*, 2001, 2003; *Lutter et al.*, 2004], body and coda wave tomography [*Eberhart-Phillips and Michael*, 1998; *Magistrale and Sanders*, 1995; *Shapiro et al.*, 2005], modeling of geodetic data [*Le Pichon et al.*, 2005] and analysis of head waves that refract along material interfaces in the fault zone structure [*McGuire and Ben-Zion*, 2005, and references therein]. The range of the velocity contrast across the San Andreas and other large faults is estimated to be about up to 30%, with values of 5-20% often reported.

A fault surrounded by identical materials on both sides cannot become unstable when the governing friction law has a single, constant coefficient of friction. However, an interface separating materials of different elastic properties can become unstable even under this condition [*Weertman*, 1980]. How much earthquake ruptures are influenced by such material contrasts has been under debate recently [*Andrews and Harris*, 2005; *Harris and Day*, 2005; *Ben-Zion*, 2006a, b]. The model of rupture propagation along a bimaterial interface with a single, constant friction coefficient evidently excludes the weakening behavior of friction during sliding and is unrealistic in this respect. Nevertheless, it is also believed that simple weakening models of friction and their parameters do not have a clean physical basis and additional physical knowledge has to be developed to come to physically consistent models [*Rice and Cocco*, 2006].

Destabilization of slip on a bimaterial interface is only present in the 2D in-plane case and it is not present in the 2D anti-plane case. It has been mentioned by *Ben-Zion and Andrews* [1998] that the results of bimaterial driven 2D in-plane rupture simulations might be modified considerably in cases of 3D rupture propagation. *Harris and Day* [2005] show results of dynamic rupture calculations in 3D with slip-weakening and Kelvin-Voigt viscosity in the bulk. However, (1) it is not yet clear that the Kelvin-Voigt viscosity does regularize ill-posedness, and (2) we wish to isolate the bimaterial instability from that coming from the intrinsic frictional weakening. Therefore the problem of a rupture along a bimaterial interface in 3D still needs examination.

2. Ill-posedness, and numerical convergence

2.1. Ill-posedness and Regularization

A frictional interface governed by Coulomb friction in a homogeneous medium with a uniform initial stress along the fault less than the frictional strength never becomes unstable no matter how forcefully an event is initiated in the nucleation zone. As mentioned above, in order to study unstable slip on a bimaterial interface independently from other sources of instability (e.g., slip- or rate-dependent friction) one would therefore ideally wish to use Coulomb friction. However, sliding along a planar bimaterial interface under Coulomb friction is often not well-posed [*Adams*, 1995; *Ranjith and Rice*, 2001] in the sense that such problems do not possess any solution, even if not-too-refined numerical simulations might appear to be stable.

It has been shown by *Ranjith and Rice* [2001] that there is a connection between the ill-posedness of the problem and the existence of the generalized Rayleigh wave. A summarizing table is given in *Cochard and Rice* [2000]. The source of ill-posedness has been studied by *Adams* [1995] and is referred to as the Adams instability [*Cochard and Rice*, 2000].

In this study we use an experimentally based constitutive law derived by *Prakash and Clifton* [1993] and *Prakash* [1998] in its simplified form [*Cochard and Rice*, 2000] with its characteristic differential equation for the shear strength τ_1^s given by:

$$\dot{\tau}_1^s = -\frac{|V| + V^*}{L}\left[\tau_1^s - f \max\left(0, -\tau_2\right)\right] \tag{1}$$

with slip velocity V, characteristic slip velocity V^*, characteristic length L, and friction coefficient f letting the shear stress τ_1 to respond gradually rather than instantaneously to an abrupt change of normal stress τ_2. It has been shown by *Ranjith and Rice* [2001] to regularize the previously discussed ill-posedness. Classical slip-weakening or rate- and state-dependent constitutive laws with strength proportional to local normal stress do not provide a regularization [*Cochard and Rice*, 2000].

2.2. Numerical convergence

Even in the well-posed regime it is numerically challenging to resolve a wrinkle-like rupture pulse travelling along a bimaterial interface, because of the above mentioned intrinsic instability of such an interface [*Cochard and Rice*, 2000; *Ben-Zion and Huang*, 2002]. To test the numerical results for their physical plausibility we strive for converging results of grid-refined simulations. In Figure 1 we show converging results achieved with the finite-difference method used in this study (details in section 3) for three levels of grid refinement ($\Delta x = 0.5, 0.25, 0.125$ m). Because of the huge computational expense we cannot accomplish further refinements or larger propagation distances at the same time. The top panel shows slip velocity as a function of time at three different points ($x_{\mathrm{pd}} = 100m, 150m, 200m$) along the in-plane direction on the fault. At about 0.03 s we see a slip pulse that corresponds to what is labeled 'supershear' in figure 2 – it has already totally disappeared at 150 m away from the nucleation. Thus, as in 2D, the main feature is the so called Weertman pulse [e.g., *Andrews and Ben-Zion*, 1997], appearing in all three stations. For the least refined grid (green curve) we can see numerical noise, especially for the station at 200 m propagation distance. The corresponding features can also be seen in the bottom panel which shows normal stress. We can see that suitable convergence is achieved for $\Delta x = 0.25$ m.

3. Numerical Model and Parameter Setup

3.1. Physical Model and Numerical Implementation

The model consists of two elastic halfspaces of different elastic properties which are coupled by a frictional interface. We use a standard 4th-order staggered-grid finite-difference technique for solving the elastic wave equations inside the elastic medium which has been described by various authors [e.g., *Igel et al.*, 1995; *Graves*, 1996]. Frictional sliding is numerically included via the stress-glut method which has been introduced by *Andrews* [1999]. To keep the simulations clean from artificial reflections caused by the finiteness of the numerical implementation of the model we use perfectly matched layers [*Marcinkovich and Olsen*, 2003] of appropriate width on all sides of the modelspace. Although *Ampuero and Dahlen* [2005] show that the elastic constants on a material discontinuity are ambiguous, we found that we could achieve the best duplication of results of *Cochard and Rice* [2000] using the harmonic mean for the elastic $c_{\mathrm{av}} = 2c_1c_2/(c_1 + c_2)$ constants and the arithmetic mean for the density $\rho_{\mathrm{av}} = (\rho_1 + \rho_2)/2$, as has been suggested elsewhere [*Moczo et al.*, 2002; *Wu and Chen*, 2003], for points on the material boundary where the elastic properties are not defined in the staggered scheme.

3.2. Nucleation

We nucleate each event in a circular symmetric way by increasing the fluid pressure in a limited space-time region. We thus prevent a propagation direction that is privileged by the nucleation procedure. Our procedure is similar to the one used by *Brietzke and Ben-Zion* [2006]. In 3D it is a spatially ring-shaped nucleation pulse with the spatial width a, expanding at the nucleation velocity v_{nuc} until the maximum radius b, which can be expressed using the geometric variables $\xi = (|r| - v_{\mathrm{nuc}}t)/a$, and $\eta = (|r| + v_{\mathrm{nuc}}t)/b - (\sqrt{a^2 + b^2}/b)$, with radius $|r| = \sqrt{y^2 + z^2}$. Within the source, the fluid pressure is given as $P_{\mathrm{f}} = P_0 \left(1 - \xi^2 - \eta^2\right)^2$, while outside this region it is zero.

3.3. Model Parameters

To make our study comparable to other numerical studies [*Cochard and Rice*, 2000; *Ben-Zion and Huang*, 2002; *Ben-Zion and Shi*, 2005] we use parameters that are similar to the ones used in those studies. The range of the investigated parameters is summarized in Table 1.

4. Results

Snapshots of slip velocity on the fault at three instances in time are shown in Figure 2 for $\Delta x = 0.25$ m. The nucleation initiates rupture phases in the subshear as well as the supershear range. The supershear part of the rupture dies out for the shown parameter set in all directions. In the in-plane direction and some time-dependent angle the subshear rupture phase develops towards a self-amplifying wrinkle-like pulse in the positive direction (direction of slip in the softer material), and it dies out in the opposite (negative) direction. This self-amplifying wrinkle-like pulse travels at about the generalized Rayleigh velocity within a limited region of slip that has the shape of a fraction of a circle. Therefore the propagation velocity of this pulse is constant in all directions where it exists. In the anti-plane direction the pulse symmetrically dies out for all propagation velocities. Although this might look trivial knowing the corresponding 2D cases, where we have the development of a unilateral rupture-pulse in the positive direction of the in-plane case, and dying rupture pulses in the anti-plane case, we want to emphasize that this result cannot be deduced trivially from the separate 2D cases. The snapshots show how a self-amplifying, purely material-contrast driven wrinkle-like rupture pulse can appear also in the 3D case. We found that the allowance of rake rotation in the 3D case does not change the results qualitatively (in a few simulations, not shown here, we found that the self-amplification is stronger for the cases for which we prohibited rake-rotation).

In order to investigate how the pulse evolves after some larger propagation distance we performed a 3D simulation with a coarse numerical grid ($\Delta x = 0.5$ m) allowing us to enlarge the propagation distance to $x_{\mathrm{pd}} = 1$ km. The resulting slip-distribution after

475 ms is shown in figure 3. The buldge of slip on the rightmost part shows a very small disturbance (< 4% of the total slip) propagating ahead of the main pulse at the same velocity, and which originates at a propagation distances of about 400 m. The non-circular rupture front in figure 3 also indicates a transition at the edge, the rupture propagation velocity being slightly smaller there.

Our results show that for adequate parameters a wrinkle-mode of rupture that is purely driven by the decrease in normal stress during slip and its positive feedback (amplification) can exist also in the 3D case. However, in 3D it appears that the wrinkle-like rupture pulse degenerates possibly faster than in 2D towards a potentially unrealistic state with a huge slip-acceleration and very small width of the pulse (sharpening).

5. Discussion

The problem of rupture on a bimaterial interface is numerically extremely challenging because of the highly unstable physical mechanism associated with it (compared to, e.g., the classical slip-weakening instability). Using finite-difference calculations we show that a self-sustained pulse can exist under the simplified Prakash-Clifton law also in 3D. Such a pulse travels inside a cone with a time-dependent angle on the fault plane around the positive in-plane direction.

How robust are the results of this study? Based on our experience in 2D and the very limited experience in 3D, we found that there exists ranges of parameters, e.g., regarding the nucleation procedure or a too low level of initial stress, for which self-sustained pulses have not been observed. Nevertheless we are confident that self-sustained propagation occurs in at least some significant neighborhood of the present parameters. However, a full parameter space study remains to be done, even in 2D.

Based on very few numerical simulations of rupture propagation along a bimaterial interface governed by slip-weakening friction *Andrews and Harris* [2005] state that this phenomenon of the wrinkle-like pulse is not important for realistic earthquake rupture. In contrast, it has been under debate recently what is a realistic and physically consistent earthquake model. Additional physical knowledge has to be developed [*Rice and Cocco*, 2006] to narrow the involved uncertainties and to evaluate physically more consistent, more realistic models of earthquake rupture; off-fault energy dissipation due to plastic strain, visco-elasticity, melt lubrication, thermal pressurization are just examples of what could be taken into account.

Our study has the clearly defined conceptual limit of a purely material driven effect. The results of recent studies on bimaterial interfaces bring in complementary insights (e.g., *Rudnicki and Rice* [2006]; *Shi and Ben-Zion* [2006]; *Brietzke and Ben-Zion* [2006]; *Rubin and Ampuero* [2006]). There are indeed good examples for which the bimaterial mechanism seems to be necessary to properly interpret the observations: *Rubin and Gillard* [2000] observed asymmetric alongstrike distribution of aftershocks on the San Andreas fault and *Dor et al.* [2006b] observed asymmetric rock damage across faults of the San Andreas system.

In order to address the question of whether or not the wrinkle-like slip pulse (or, more generally, the bimaterial mechanism) is relevant in existing earthquake rupture mechanisms, a much wider range of models and parameter combinations would need to be tested, owing to the aforementioned uncertainties in our knowledge of source physics. The strong self-sharpening behavior of the wrinkle-like rupture pulse suggests that, with increasing propagation distance, it degenerates towards unrealistically large slip velocities (as already noted by *Ben-Zion and Huang* [2002] in 2D), and perhaps vanishes as a consequence of pulse thinning, this latter aspect obviously deserving a deeper investigation.

Acknowledgments. We are extremely grateful to Eric Dunham who reviewed and criticized the manuscript very constructively, and we thank an anonymous reviewer for helping us improving the presentation. We would also like to thank Michael Ewald, Toni Kraft, and František Gallovič for useful discussions. We thank the NBW-Konwihr project, and the Leibniz-Rechenzentrum München (LRZ) for supplying the computing facilities, Reinhold Bader for the support of the software development, the NBW-Konwihr project, the Human Ressources Mobility Program (SPICE-Project), and Munich Reinsurance for the financial support. Alain Cochard also acknowledges partial support from ANR "MODALSIS".

References

Adams, G. G., Self-excited oscillations of two elastic half-spaces sliding with a constant coefficient of friction, *ASME Journal of Applied Mechanics*, *62*, 867–872, 1995.

Ampuero, J. P., and F. A. Dahlen, Ambiguity of the Moment Tensor, *Bull. Seism. Soc. Am.*, *95*(2), 390–400, doi:10.1785/0120040103, 2005.

Andrews, D. J., Test of two methods for faulting in finite difference calculations, *Bull. Seism. Soc. Am.*, *89*(4), 931–937, 1999.

Andrews, D. J., and Y. Ben-Zion, Wrinkle-like slip pulse on a fault between different materials, *J. Geophys. Res.*, *102*, 553–572, doi:10.1029/96JB02856, 1997.

Andrews, D. J., and R. A. Harris, The wrinkle-like slip pulse is not important in earthquake dynamics, *Geophys. Res. Lett.*, *32*, 23,303–+, doi:10.1029/2005GL023996, 2005.

Ben-Zion, Y., A comment on the wrinkle-like slip pulse is not important in earthquake dynamics by Andrews and Harris, *Geophys. Res. Lett.*, *33*, L06,310, doi: 10.1029/2005GL025372, 2006a.

Ben-Zion, Y., A comment on material contrast does not predict earthquake rupture propagation direction by Harris and Day, *Geophys. Res. Lett.*, *33*, L13,310, doi: 10.1029/2005GL025652, 2006b.

Ben-Zion, Y., and D. J. Andrews, Properties and implications of dynamic rupture along a material interface, *Bull. Seism. Soc. Am.*, *88*(4), 1085–1094, 1998.

Ben-Zion, Y., and Y. Huang, Dynamic rupture on an interface between a compliant fault zone layer and a stiffer surrounding solid, *J. Geophys. Res.*, *107*, 6–1, doi: 10.1029/2001JB000254, 2002.

Ben-Zion, Y., and Z. Shi, Dynamic rupture on a material interface with spontaneous generation of plastic strain in the bulk, *Earth Planet. Sci. Lett.*, *236*, 486–496, doi: 10.1016/j.epsl.2005.03.025, 2005.

Brietzke, G. B., and Y. Ben-Zion, Examining tendencies of in-plane rupture to migrate to material interfaces, *Geophys. J. Int.*, *167*(2), 807–+, doi:10.1111/j.1365-246X.2006.03137.x, 2006.

Cochard, A., and J. R. Rice, Fault rupture between dissimilar materials: Ill-posedness, regularization, and slip-pulse response, *J. Geophys. Res.*, *105*, 25,891–25,908, doi: 10.1029/2000JB900230, 2000.

Dor, O., Y. Ben-Zion, T. K. Rockwell, and J. Brune, Pulverized rocks in the mojave section of the san andreas fault zone, *Earth Planet. Sci. Lett.*, *245*, 642–654, 2006a.

Dor, O., T. K. Rockwell, and Y. Ben-Zion, Geologic observations of damage asymmetry in the structure of the San Jacinto, San Andreas and Punchbowl faults in southern california: A possible indicator for preferred rupture propagation direction, *Pure Appl. Geophys.*, *163*, 301–349, doi:10.1007/s00024-005-0023-9, 2006b.

Eberhart-Phillips, D., and A. J. Michael, Seismotectonics of the Loma Prieta, California, region determined from three-dimensional v_p, v_p/v_s, and seismicity, *J. Geophys. Res.*, *103*, 21,009–21,120, 1998.

Fuis, G. S., T. Ryberg, N. Godfrey, D. A. Okaya, and J. Murphy, Crustal structure and tectonics from the Los Angeles basin to the Mojave desert, southern ca, *Geology*, *29*, 15–18, 2001.

Fuis, G. S., R. W. Clayton, P. M. Davis, W. J. Ryberg, T. Lutter, D. A. Okaya, E. Hauksson, C. Prodehl, J. M. Murphy, M. L. Benthien, S. A. Baher, M. D. Kohler, K. Thygesen, G. Simila, and G. R. Keller, Fault systems of the 1971 San Fernando and 1994 Northridge earthquakes, southern California: Relocated aftershocks and seismic images from LARSE II, *Geology*, *31*, 171–174, 2003.

Graves, R. W., Simulating seismic wave propagation in 3D elastic media using staggered-grid finite differences, *Bull. Seism. Soc. Am.*, *86*(4), 1091–1106, 1996.

Harris, R. A., and S. M. Day, Material contrast does not predict earthquake rupture propagation direction, *Geophys. Res. Lett.*, *Vol. 32*, L23,301, doi:10.1029/2005GL023941, 2005.

Igel, H., P. Mora, and B. Riollet, Anisotropic wave propagation through finite-difference grids, *Geophysics*, *60*(4), 1203–1216, doi:10.1190/1.1443849, 1995.

Le Pichon, X., C. Kreemer, and N. Chamot-Rooke, Asymmetry in elastic properties and the evolution of large continental strike-slip faults, *Journal of Geophysical Research (Solid Earth)*, *110*, 3405–+, doi:10.1029/2004JB003343, 2005.

Lutter, W. J., G. S. Fuis, T. Ryberg, D. A. Okaya, R. W. Clayton, P. M. Davis, C. Prodehl, J. M. Murphy, V. E. Langenheim, M. L. Benthien, N. J. Godfrey, N. I. Christensen, K. Thygesen, C. H. Thurber, G. Simila, and G. R. Keller, Upper crustal structure from the Santa Monica mountains to the Sierra Nevada, southern California: tomographic results from the Los Angeles regional seismic experiment, phase ii (LARSE)., *Bull. Seism. Soc. Am.*, *94*(2), 619–632, doi:10.1785/0120030058, 2004.

Magistrale, H., and C. Sanders, P-wave image of the Peninsular Ranges batholith, southern California, *Geophys. Res. Lett.*, *22*, 2549–2552, 1995.

Marcinkovich, C., and K. Olsen, On the implementation of perfectly matched layers in a three-dimensional fourth-order velocity-stress finite difference scheme, *Journal of Geophysical Research (Solid Earth)*, *108*, doi:10.1029/2002JB002235, 2003.

McGuire, J., and Y. Ben-Zion, High-resolution imaging of the Bear Valley section of the San Andreas Fault at seismogenic depths with fault-zone head waves and relocated seismicity, *Geophys. J. Int.*, *163*, 152–164, doi:10.1111/j.1365-246X.2005.02703.x, 2005.

Moczo, P., J. Kristek, V. Vavrycuk, R. J. Archuleta, and L. Halada, 3D Heterogeneous Staggered-Grid Finite-Difference Modeling of Seismic Motion with Volume Harmonic and Arithmetic Averaging of Elastic Moduli and Densities, *Bull. Seism. Soc. Am.*, *92*(8), 3042–3066, doi:10.1785/0120010167, 2002.

Prakash, V., Frictional response of sliding interfaces subjected to time varying normal pressures, *J. of Tribol.*, *120*, 97–102, 1998.

Prakash, V., and R. J. Clifton, *Time resolved dynamic friction measurements in pressure-shear*, *Appl. Mech. Div.*, vol. 165, pp. 33–48, ASME, New York, 1993.

Ranjith, K., and J. Rice, Slip dynamics at an interface between dissimilar materials, *J. Mach. Phys. Solids*, *49*, 341–361, 2001.

Rice, J. R., and M. Cocco, *The Dynamics of Fault Zones*, *Dahlem Workshop Reports*, vol. 95, chap. Seismic fault rheology and earthquake dynamics, pp. 1–36, The MIT Press, Cambridge, MA, USA, 2006.

Rubin, A. M., and J. P. Ampuero, Aftershock asymmetry on a bimaterial interface, *J. Geophys. Res.*, *submitted*, 2006.

Rubin, A. M., and D. Gillard, Aftershock asymmetry/rupture directivity among central San Andreas fault microearthquakes, *J. Geophys. Res.*, *105*, 19,095–19,109, 2000.

Rudnicki, J. W., and J. R. Rice, Effective normal stress alteration due to pore pressure changes induced by dynamic slip propagation on a plane between dissimilar materials, *J. Geophys. Res.*, *111*, B10,308, doi:10.1029/2006JB004396, 2006.

Shapiro, N. M., M. Campillo, L. Stehly, and M. H. Ritzwoller, High resolution surface wave tomography from ambient seismic noise, *Science*, *307*, 1615–1618, 2005.

Shi, Z., and Y. Ben-Zion, Dynamic rupture on a bimaterial interface governed by slip-weakening friction, *Geophys. J. Int.*, *165*, 469–484, doi:10.1111/j.1365-246X.2006.02853.x, 2006.

Weertman, J. J., Unstable slippage across a fault that separates elastic media of different elastic constants, *J. Geophys. Res.*, *85*, 1455–1461, doi: 10.1029/0JGREA0000850000B3001455000001, 1980.

Wu, Z. L., and Y. T. Chen, Definition of Seismic Moment at a Discontinuity Interface, *Bull. Seism. Soc. Am.*, *93*(4), 1832–1834, doi:10.1785/0120020234, 2003.

Table 1. Range of simulation parameters

parameter	value or value range
numerical method	finite-differences
grid type	staggered cartesian grid
grid-spacing Δx	0.5 m, 0.25 m, 0.125 m
maximum grid size $n_x \times n_y \times n_z$	$500 \times 3200 \times 3200$
maximum size of the physical model $x \times y \times z$	$230 \times 1580 \times 1580$ m^3
density material 1 ρ_1	3333.3 kg/m^3
wave velocities material 1 v_{s1}, v_{p1}	3000.0, 5196.2 m/s
density material 2 ρ_2	2777.7 kg/m^3
wave velocities material 2 v_{s2}, v_{p2}	2500.0, 4330.1 m/s
size of the fault model $y \times z$	$1580 \times 1580 = 2496400$ m^2
type of friction	simplified Prakash-Clifton
friction coefficient f	0.75
characteristic slip velocity V^*	1 m/s
characteristic length L	4 mm
initial shear stress τ^∞	70 MPa
initial normal stress σ^∞	100 MPa
size of nucleation zone $\oslash_{\mathrm{nuc}} = 2b$	120 m
nucleation velocity v_{nuc}	2475 m/s
nucleation pulse width a	10 m

Figure 1. Slip velocity, shear-stress, friction, and normal stress at three stations at 100 m, 150 m and 200 m propagation distance along the in-plane direction for the parameter case shown in table 1. For the shown propagation distances, a resolution of $\Delta x = 0.25$ m provides already good convergence, since the results of the next refinement with $\Delta x = 0.125$ m basically shows the same solution.

Figure 2. Snapshots of the slip velocity on the fault-plane at three instances in time for the same parameters as in figure 1. The nucleation takes place inside the pink circle ($\oslash_{\text{nuc}} = 2b = 120$ m). The left panel shows slip velocity shortly after the nucleation. Two supershear half-moon shaped rupture phases, and a subshear rupture phase traveling at about the generalized Rayleigh velocity in all directions (see left panel) are initiated. The subshear rupture phase develops towards a self-amplifying wrinkle-like pulse within a cone around the positive in-plane direction, it dies out in the negative in-plane as well as in the anti-plane directions (see middle/right panel).

Figure 3. Distribution of slip after 475 ms simulation time. After passing the nucleation region at $r_{\text{pd}} < 60$ m the pulse travels through a transitional area of relatively stable pulse propagation (compare with figure 2) until it becomes clearly self-sustained.

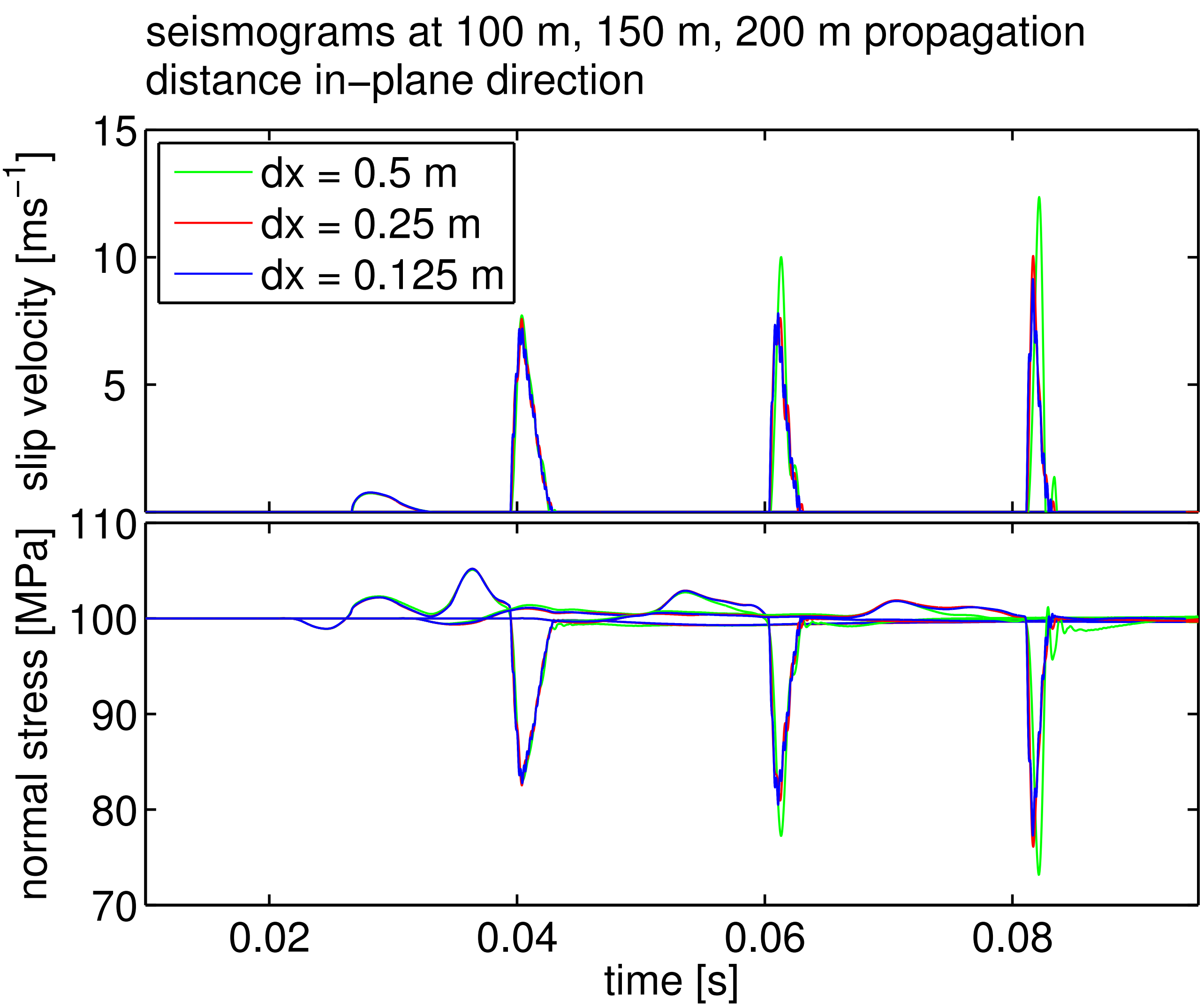
seismograms at 100 m, 150 m, 200 m propagation
distance in−plane direction
dx = 0.5 m
dx = 0.25 m
dx = 0.125 m
slip velocity [ms−1]
normal stress [MPa]
15
10
5
110
100
90
80
70
0.02
0.04
0.06
0.08
time [s]

Figure 1.

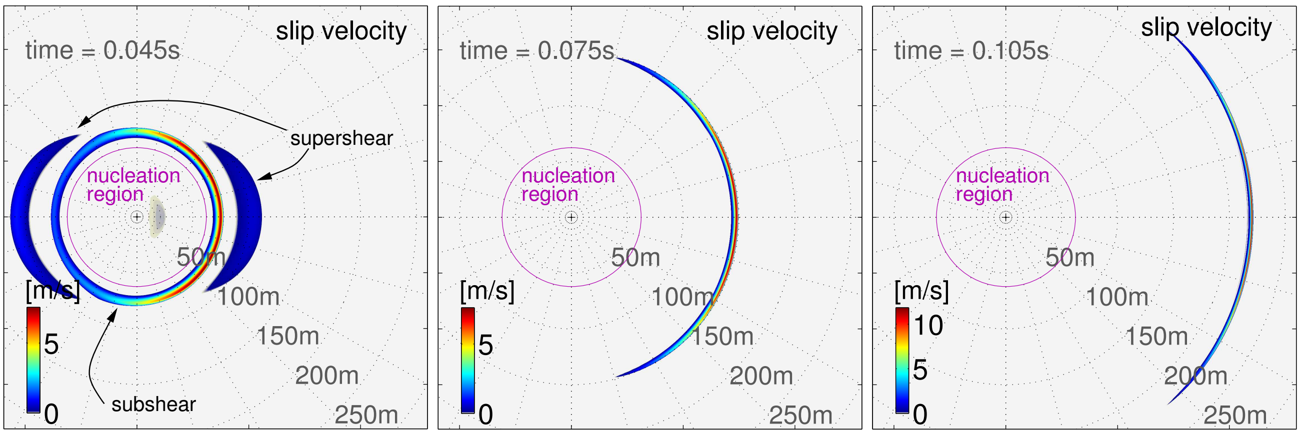
time = 0.045s
slip velocity
supershear
nucleation region
50m
100m
150m
200m
250m
[m/s]
5
0
subshear
time = 0.075s
slip velocity
nucleation region
50m
100m
150m
200m
250m
[m/s]
5
0
time = 0.105s
slip velocity
nucleation region
50m
100m
150m
200m
250m
[m/s]
10
5
0

Figure 2.

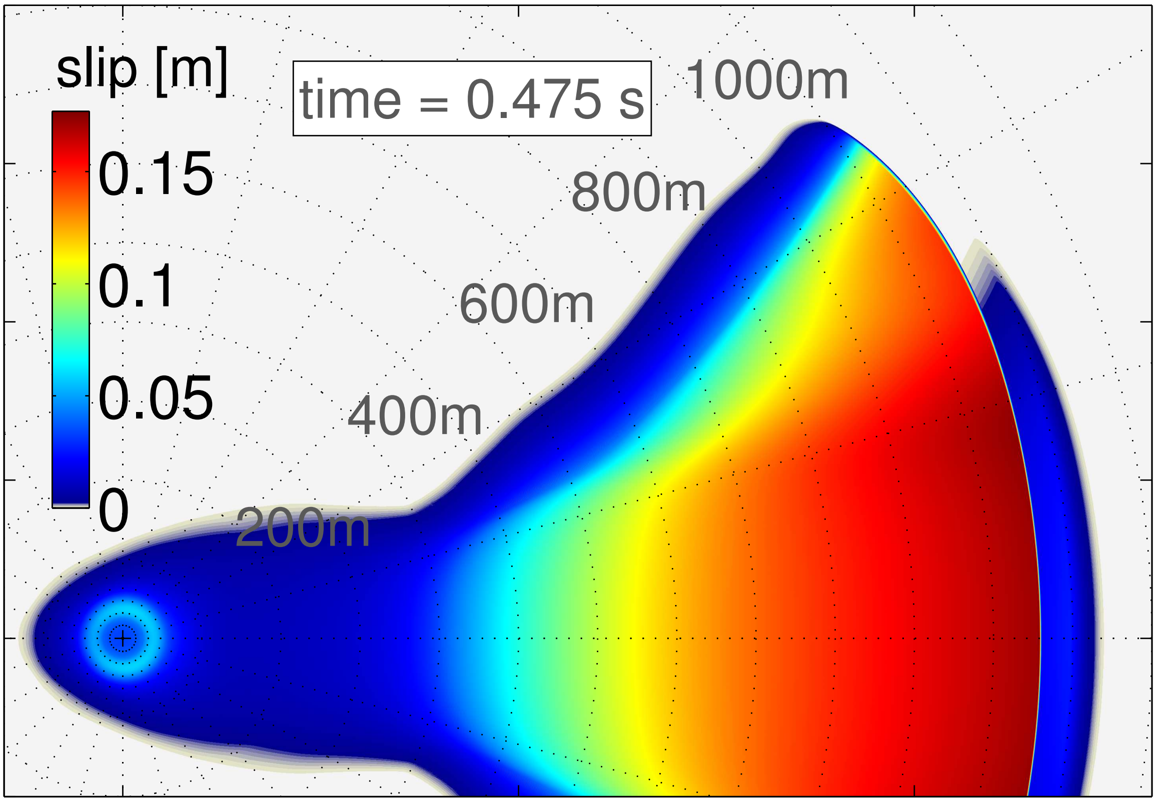

Figure 3.